HHS Public Access

Author manuscript

Ann Neurol. Author manuscript; available in PMC 2022 January 03.

Published in final edited form as:

Ann Neurol. 2019 August ; 86(2): 279–292. doi:10.1002/ana.25512.

Different microvascular alterations underlie microbleeds and microinfarcts

Susanne J. van Veluw, PhD[1,2], **Ashley A. Scherlek, BM**[1], **Whitney M. Freeze, PhD**[1,3], **Annemieke ter Telgte, MSc**[1,4], **Andre J. van der Kouwe, PhD**[5], **Brian J. Bacskai, PhD**[1], **Matthew P. Frosch, MD PhD**[1,6], **Steven M. Greenberg, MD PhD**[2]

[1]MassGeneral Institute for Neurodegenerative Disease, Massachusetts General Hospital and Harvard Medical School, Charlestown, MA, USA

[2]J. Philip Kistler Stroke Research Center, Department of Neurology, Massachusetts General Hospital and Harvard Medical School, Boston, MA, USA

[3]Department of Psychiatry and Neuropsychology, Maastricht University, School for Mental Health and Neuroscience, Alzheimer Center Limburg, Maastricht, the Netherlands

[4]Department of Neurology, Donders Institute for Brain, Cognition and Behaviour, Radboud University Medical Center, Nijmegen, the Netherlands

[5]Athinoula A. Martinos Center for Biomedical Imaging, Department of Radiology, Massachusetts General Hospital, Charlestown, MA, USA

[6]Neuropathology Service, C.S. Kubik Laboratory for Neuropathology, Massachusetts General Hospital and Harvard Medical School, Boston, MA, USA

Abstract

Objective: Cerebral amyloid angiopathy (CAA) is characterized by the accumulation of amyloid β (Aβ) in the walls of cortical vessels and the accrual of microbleeds and microinfarcts over time. The relationship between CAA severity and microbleeds and microinfarcts as well as the sequence of events that lead to lesion formation remain poorly understood.

Methods: We scanned intact formalin-fixed hemispheres of 12 CAA cases with MRI, followed by histopathological examination in pre-defined areas and serial sectioning in targeted areas with multiple lesions.

Results: In total 1,168 cortical microbleeds and 472 cortical microinfarcts were observed on *ex vivo* MRI. Increasing CAA severity at the whole-brain or regional level was not associated with the number of microbleeds or microinfarcts. However, locally, the density of Aβ positive cortical vessels was lower surrounding a microbleed compared to a simulated control lesion, and higher

Corresponding author: Susanne van Veluw, Massachusetts General Hospital, MassGeneral Institute for Neurodegenerative Disease, 114 16th Street, Charlestown, MA 02129, USA, svanveluw@mgh.harvard.edu.

Author contributions

SJvV, BJB, MPF, and SMG contributed to the conception and design of the study; SJvV, AAS, WMF, AtT, AvdK, and MPF contributed to the acquisition and analysis of the data; SJvV drafted the text and prepared the figures.

Potential conflicts of interest

Nothing to report.

surrounding microinfarcts. Serial sectioning revealed that for (n=28) microbleeds both Aβ (4%) and smooth muscle cells (4%) were almost never present in the vessel wall at the site of bleeding, but Aβ was frequently observed upstream or downstream (71%), as was extensive fibrin(ogen) build-up (87%). In contrast, for (n=22) microinfarcts vascular Aβ was almost always observed at the core of the lesion (91%, p<0.001) as well as upstream or downstream (82%), but few vessels associated with microinfarcts had intact smooth muscle cells (9%).

Interpretation: These observations provide a model for how a single neuropathologic process such as CAA may result in hemorrhagic or ischemic brain lesions potentially through two different mechanistic pathways.

Introduction

Cerebral amyloid angiopathy (CAA) is an age-related cerebral small vessel disease that commonly affects the brains of older individuals[1]. Traditionally, CAA has been considered primarily a bleeding disorder based on the observation of multiple microbleeds on brain scans of affected patients and the occurrence of symptomatic lobar intracerebral hemorrhage (ICH)[1,2]. More recently, it has become clear that widespread ischemic brain tissue injuries such as white matter hyperintensities and microinfarcts are also prominent features in CAA, most likely contributing to gradual cognitive decline in these patients[3–5]. Even though hemorrhagic lesions (*e.g.* microbleeds) and ischemic lesions (*e.g.* microinfarcts) commonly co-occur in patients with CAA it remains largely unknown if they share similar or distinct underlying pathophysiological pathways. Neuropathologically, CAA is characterized by the accumulation of the amyloid β (Aβ) peptide in the walls of leptomeningeal and cortical arterioles, which is believed to be the main cause for microbleed and microinfarct formation in affected areas[6]. Yet, there are few studies that have directly assessed the relationship between CAA burden and the occurrence of microbleeds and microinfarcts throughout the brain. Moreover, the exact underlying sequence of events in a single vessel that lead to either a microbleed or a microinfarct in patients with CAA are not fully understood. To fill this gap, we used high-resolution *ex vivo* MRI combined with histopathology in intact hemispheres to assess the associations between microbleeds and microinfarcts with CAA severity at the whole-brain, regional, and local level. Furthermore, guided by *ex vivo* MRI, we sampled lesion-rich areas to perform serial sectioning to assess the pathology of microbleeds and microinfarcts at the single-vessel level. Recently, in an exploratory study of single histopathological sections of MRI-targeted microbleeds in areas with severe CAA, we reported absence of Aβ from the wall of the bleeding arterioles at the site of rupture[7]. This observation leads to the question whether microbleeds in CAA happen 1) because of extensive remodeling of the arteriolar wall (including loss of Aβ) or 2) in healthy vessels without Aβ that are perhaps more at risk to ‘take the hit’ when the local CAA-affected network (likely stiffened) is under pressure. In this study, we aimed to answer these questions using serial sectioning to uncover the properties of the vessels involved in microbleeds both at the site of rupture as well as upstream and downstream. Moreover, we aimed to extend these observations to microinfarcts, for which the relationship with vascular Aβ is currently unknown.

Methods

Cases

Thirteen intact brains were received through an ongoing brain donation program initiated within the hemorrhagic stroke research group at the Massachusetts General Hospital (MGH) aimed at the evaluation of MRI markers and their underlying histopathology in the context of CAA[8,9]. All cases had received a clinical diagnosis of possible or probable CAA during life[1]. At autopsy, brains were extracted and fixed in 10% formalin for several weeks, after which the hemispheres were separated by a single midsagittal cut. The least affected hemisphere was used for *ex vivo* MRI scanning and histopathology in the context of this study. The other hemisphere was processed to undergo routine neuropathological examination by a board-certified neuropathologist. One case was excluded from further analysis, because no evidence of CAA was found on routine neuropathological examination. Study approval was received from the MGH institutional review board and informed consent was obtained from the next of kin or another legal representative prior to autopsy.

Study design

The experimental design of the study is depicted in Fig.1. First, intact formalin-fixed hemispheres were subjected to high-resolution *ex vivo* 3 tesla (T) MRI to detect microbleeds and microinfarcts. Next, the hemispheres were cut in 10 mm-thick coronal slabs and standard samples were taken from pre-defined areas of frontal, temporal, parietal, and occipital cortex. Four adjacent 6 μm-thick sections were cut from these samples and stained with hematoxylin & eosin (H&E), Luxol fast blue H&E, Aβ, and glial fibrillary acidic protein (GFAP) to assess regional associations between histopathologically-observed microbleeds and microinfarcts and CAA severity. A composite CAA severity score was calculated to assess whole-hemisphere associations between MRI-observed microbleeds and microinfarcts and CAA severity. Finally, three additional samples were taken from three cases in an area with multiple microbleeds (from temporal cortex from case #2 and #10) or microinfarcts (from parieto-occipital cortex from case #4) that were visible on *ex vivo* 3T MRI. Samples from case #2 and #4 underwent ultra-high-resolution *ex vivo* 7T MRI scanning to confirm the high number of lesions in those areas. Afterwards, all three samples underwent complete serial sectioning (6 μm-thick sections) to ensure that all lesions were captured. Sections 1, 21, 41, 61 etc. were stained with H&E to identify microbleeds and microinfarcts, and sections 2, 6, 10, 14 etc. underwent immunohistochemistry against Aβ. These serial sections were used to assess local and single-vessel associations between microbleeds and microinfarcts and CAA severity. If present, the vessel that could be traced through the core of the lesion was identified as the presumed ‘culprit’ vessel. In addition, for each identified lesion on H&E, spare adjacent sections underwent immunohistochemistry to detect fibrin(ogen) or smooth muscle cells (SMCs).

Ex vivo MRI scanning

The hemisphere to undergo *ex vivo* 3T MRI was prepared and scanned as described previously[8]. Briefly, it was packed in a plastic bag filled with periodate-lysine-paraformaldehyde (PLP) and vacuum sealed to remove air bubbles. Next, it was placed in the 32-channel head coil of a whole-body 3T MRI scanner (MAGNETOM Trio, Siemens

Healthineers, Erlangen, Germany) and scanned with an overnight protocol, including a T2-weighted turbo-spin echo (TSE) sequence (resolution 500x500x500 μm^3) and a gradient-echo fast low angle shot (FLASH) sequence (resolution 500x500x500 μm^3).

The two smaller samples to undergo *ex vivo* 7T MRI were prepared and scanned as described previously[10]. Briefly, each sample was placed in a 50 mL falcon tube, submerged in Fomblin (Solvay Solexis, Thorofare, New Jersey) and placed in a custom-built solenoid coil and scanned on a whole-body 7T MRI scanner (MAGNETOM, Siemens Healthineers). The overnight protocol included a T2-weighted TSE sequence (resolution 100x100x100 μm^3) and a FLASH sequence (resolution 75x75x75 μm^3).

Ex vivo MRI analysis

Scans were processed in FreeSurfer (https://surfer.nmr.mgh.harvard.edu) to obtain 3D volumes[11]. Microbleeds and microinfarcts were assessed blinded to CAA severity or other histopathologic findings as previously described[10]. Briefly, cortical microbleeds were identified on the gradient-echo and T2-weighted images, appearing as homogeneous round or ovoid foci of low signal intensity. Cortical microinfarcts were identified on the T2-weighted images, appearing as hyperintense foci within the cortical ribbon. Lesions were annotated using an in-house developed tool, incorporated in MeVisLab (MeVis Medical Solutions AG, Bremen, Germany). To obtain 3D visualizations of the topographical localization of microbleeds and microinfarcts within each case, annotations were projected on surface renderings of each individual hemisphere.

Histopathology

Samples taken from pre-defined standard areas of frontal, temporal, parietal, and occipital cortex and the additional samples that were taken from three cases in an area with multiple lesions were processed and embedded in paraffin, after which 6 μm-thick sections were cut on a microtome. H&E and Luxol fast blue H&E staining was performed using standard histology protocols. Bright field immunohistochemistry against Aβ (mouse, clone 6F/3D, Agilent, 1:200), GFAP (rabbit, G9269, Sigma, 1:1,000), and fibrin(ogen) (rabbit, Dako, 1:500) was performed as described previously[8,9]. To assess SMCs, sections underwent fluorescent immunohistochemistry to visualize Aβ (rabbit, IBL, 1:500 and anti-rabbit Alexa Fluor 350 (1:250) as the secondary), SMCs (mouse, Dako, 1:250 and anti-mouse Alexa Fluor 488 (1:500) as the secondary), and endothelial cells (DyLight 594-labeled Lycopersicon Esculentum (Tomato) Lectin, Vector Laboratories, 1:500) within the same vessel. Negative controls were included by omitting the primary antibodies and showed no immunopositivity.

Histopathology image analysis

Digital brightfield microscopic images of the sections were obtained with the Hamamatsu NanoZoomer Digital Pathology (NDP)-HT whole slide scanner (C9600-12, Hamamatsu Photonics KK, Japan) equipped with a 20x objective. The software NDP.View2 (version 2.7.25) was used to assess the obtained digital images. Fluorescent microscopic images were obtained with a Zeiss fluorescent microscope and a 5x objective.

Microbleeds and microinfarcts were identified on the H&E-stained sections, using the following criteria. Any area of extravasated (lysed) red blood cells with or without hematoidin was classified as an acute/recent microbleed. A few hemosiderin deposits at the edges of the lesion were allowed. An area with many focal hemosiderin deposits with or without evidence of hematoidin was classified as an old/chronic microbleed[12]. Recent/acute microinfarcts were considered areas of tissue pallor with evidence of 'red' (*i.e.* hypoxic) neurons. Old/chronic microinfarcts were characterized by tissue loss with cavitation or 'puckering' and GFAP positivity around the edges of the lesion[5]. CAA severity was evaluated on the Aβ-stained sections from the pre-defined standard areas of frontal, temporal, parietal, and occipital cortex using a 4-point scale; absent (0), scant Aβ deposition (1), some circumferential Aβ (2), widespread circumferential Aβ (3), following proposed consensus criteria[13]. Scores from the four areas were added to form a cumulative CAA severity score (Table 1).

Sholl analysis was performed to assess local CAA burden surrounding microbleeds and microinfarcts, as described previously[7]. From the serial sections from three cases, annotated microbleeds and microinfarcts on the H&E-stained sections were included, except when they were located close to another lesion or to an edge of the section. On each section, two control areas were selected on H&E (blinded for CAA severity), in a local area without a lesion. Each lesion or control area was localized on the adjacent Aβ-stained section and images were exported at 2.5x magnification. Each lesion was covered with a round or oval shaped mask in Paint. The same size and shape masks were used for the accompanying control areas to ensure blinding for lesion presence. Sholl analyses were performed >1 week on de-identified images in an in-house developed interface incorporated in MeVisLab (MeVis Medical Solutions AG). Markers were placed in the center of Aβ positive cortical vessels. The cortical ribbon was manually outlined and the resulting area surrounding the masks was divided into four concentric shells (each shell measuring 100 pixels in width, which equals 360 μm). In each shell, the density of Aβ positive cortical vessels / mm^2 was calculated. Microbleed size was calculated by measuring the greatest diameter on the H&E section that captured the center of the lesion.

From the same serial sections, all microbleeds and microinfarcts that were annotated on the H&E-stained sections were included for the single-vessel analysis. All stained sections (*i.e.* H&E, Aβ, fibrin(ogen), SMC/Aβ/lectin) surrounding a microbleed or microinfarct were visually inspected to determine whether the presumed 'culprit' vessel was visible and to determine presence or absence of Aβ, fibrin(ogen), or SMCs in the wall of the 'culprit' vessel at the lesion site or in the same vessel upstream or downstream from the lesion site. Because immunohistochemistry against Aβ was performed on section 2, 6, 10, 14 etc. individual vessels could be traced to determine the presence or absence of Aβ in detail.

Statistical analysis

Correlations for the whole-hemisphere and regional analyses were calculated using Spearman's rank correlation coefficients. The CAA severity scores in occipital and parietal cortex (posterior brain areas) and frontal and temporal cortex (anterior brain areas) were averaged and compared with a Wilcoxon signed-rank test for within-case comparisons.

Group differences in density of Aβ positive cortical vessels for the local Sholl analyses were calculated using Mann-Whitney U tests. The two samples from case #2 and #10 were analyzed separately from the sample from case #4 as they were taken from different anatomical areas of the brain. Differences between diameter of old/chronic and recent/acute microbleeds were calculated with an independent samples t-test. A χ-square test was used to determine whether microinfarcts had more often Aβ in the walls of vessels at the site of rupture compared to microbleeds. Graphs were generated in Graphpad Prism (version 5.03), and statistical analyses were performed in SPSS (version 22, IBM).

Results

Whole-hemisphere associations

The brains of 12 autopsy cases (8 males, 4 females; mean age at death 73 years [range 64-88]) that met the Boston criteria for definite CAA[1] were included in this study (Table 1). The median cumulative CAA severity score was 7.5 [range 5-10 out of a max score of 12]. On *ex vivo* 3T MRI a total number of 1,168 cortical microbleeds (mean 97±88 per case, range 4-261) and 472 cortical microinfarcts (mean 39±46 per case, range 3-144) were observed (Fig.2A B). Microbleeds were more often observed in posterior parts of the brain, whereas microinfarcts frequently involved the parts of the brain perfused by end arteries (Fig.2C). Neither the number of microbleeds (Spearman's ρ 0.426, p=0.17) nor the number of microinfarcts (Spearman's ρ −0.278, p=0.38) on *ex vivo* 3T MRI correlated with cumulative CAA severity score (Fig.2D E F). However, cases with >80 microbleeds on *ex vivo* 3T MRI (n=6) did have more severe CAA compared to cases with <80 microbleeds (n=6) (p=0.050).

Regional associations

Given the relatively weak association between microbleeds and microinfarcts and CAA severity at the whole-hemisphere level, we next asked the question whether microbleeds and microinfarcts were more often observed in regional areas with higher CAA severity. To this end, we assessed microbleeds and microinfarcts histopathologically to correlate directly with CAA severity on the same section. On the H&E-stained sections taken from pre-defined areas from frontal, temporal, parietal, and occipital cortex a total number of 13 cortical microbleeds were observed across cases (mean 1.1±1.3 [range 0-4] per case for all areas combined) and 94 cortical microinfarcts (mean 7.8±7.5 [range 0-21]) (Fig.3A). The number of microbleeds on *ex vivo* 3T MRI correlated with the total number of microbleeds on histopathology (Spearman's ρ 0.572, p=0.052), whereas microinfarcts did not (Spearman's ρ 0.452, p=0.14). CAA severity was significantly greater in posterior (occipital and parietal) compared to anterior brain areas (frontal and temporal) (Fig.3B, p=0.005). The number of microbleeds and microinfarcts observed on the H&E-stained sections did not correlate with CAA severity in any area examined (*i.e.* frontal, temporal, parietal, and occipital cortex), except for a negative correlation between CAA severity and the number of microinfarcts in parietal cortex (Spearman's ρ −0.630, p=0.028). Also, in line with the whole-hemisphere associations described above, neither the total number of microbleeds (Spearman's ρ 0.124, p=0.701) nor the total number of microinfarcts (Spearman's ρ −0.379, p=0.225) on histopathology from all areas combined correlated with cumulative CAA severity score.

In the characterization of the lesions, out of the total number of 94 microinfarcts, 61 (65%) were considered old/chronic and 33 (35%) recent/acute (Fig.3C D). Two old/chronic microinfarcts showed some evidence of hemorrhagic transformation. With respect to localization, 46 (49%) (31 old, 15 recent) followed the perfusion area of a penetrating cortical arteriole, whereas 48 (51%) (30 old, 18 recent) were located deeper (within layer III-VI) in the cortex. The correlations with regional CAA severity did not notably change when analyzing old/chronic and recent/acute microinfarcts separately.

Out of the total number of 13 microbleeds, 12 (92%) were considered old/chronic, and 1 (8%) recent/acute (Fig.3E). In terms of localization, 10 (77%) (9 old, 1 recent) followed the perfusion area of a penetrating cortical arteriole, whereas 3 (23%) were located deeper (within layer III-VI) in the cortex.

Local associations

We next asked whether microbleeds or microinfarcts occurred more often in areas with increased CAA severity in the immediate surrounding area. For this analysis, we used the serial sections taken from the temporal cortex in two CAA cases (#2 and #10) with many microbleeds in those areas as observed on *ex vivo* 3T MRI (confirmed with *ex vivo* 7T MRI). Notably, serial sectioning revealed that microinfarcts were present in these samples as well. As such, a total number of 28 microbleeds (14 old/chronic, 14 recent/acute), 18 microinfarcts (16 old/chronic, 2 recent/acute) and 80 control areas were analyzed (Fig.4A B). Significantly fewer Aβ positive cortical vessels were observed in the first shell immediately surrounding a microbleed (1.2±1.8 vessels / mm^2) compared to a simulated control lesion (2.0±2.0 vessels / mm^2, p=0.023), whereas more Aβ positive cortical vessels were observed in the first shell immediately surrounding a microinfarct compared to a simulated control lesion (3.2±2.5 vessels / mm^2, p=0.054) (Fig.4C D) (each shell is a progressive 360 μm area surrounding a lesion). The difference between microbleeds and simulated control lesions in shell 1 was driven by old/chronic microbleeds (p=0.004) and not recent/acute microbleeds (p=0.57), which became clear after analyzing them separately. Of note, for old/chronic microbleeds shell 2 also contained significantly fewer Aβ positive cortical vessels compared to simulated control lesions (p=0.043). This may be the result of the observation that recent/acute microbleeds were significantly larger (greatest diameter on H&E: 986±554 μm) compared to old/chronic microbleeds (greatest diameter on H&E: 397±268 μm, p=0.002) and therefore the immediate surrounding area of a recent/acute microbleed was likely still occupied with extravasated red blood cells.

To similarly assess local CAA severity surrounding recent/acute microinfarcts (as opposed to old/chronic microinfarcts that were more abundant in the analysis above) we analyzed an independent sample from the parieto-occipital cortex in a third CAA case (#4) with many recent/acute microinfarcts in that area as observed on *ex vivo* 3T MRI (confirmed with *ex vivo* 7T MRI). A total number of 11 recent/acute microinfarcts and 28 control areas from these serial sections were analyzed independently. Significantly more Aβ positive cortical vessels were observed in the first shell immediately adjacent to a recent/acute microinfarct (4.6±4.8 vessels / mm^2) compared to a simulated control lesion (1.9±2.0

vessels / mm^2, p=0.031) (Fig.6). These findings suggest that microinfarcts occur in local areas with increased CAA severity.

Single-vessel associations

Finally, we aimed to assess the feeding vessel of each microbleed and microinfarct captured on the serial sections to determine the pathological changes at the level of the individual vessel that presumably caused the lesion. A total number of 28 microbleeds (14 old/chronic, 14 recent/acute) from two cases, and 22 microinfarcts (15 old/chronic, 7 recent/acute) from three cases were analyzed. The findings from old/chronic and recent/acute lesions were comparable and hence are summarized together. The culprit vessel could be reliably identified in 24 out of 28 microbleeds (86%). Aβ was observed in the vessel wall at the rupture site for only 1 (4%) microbleed, whereas Aβ was observed in the vessel wall upstream or downstream for 20 (71%) microbleeds. In 20 out of 23 (87%) available culprit vessels extensive fibrin(ogen) was present in the wall at the lesion site (the other 3 vessels showed mild fibrin(ogen) deposition). Intact SMCs at the lesion site were observed for only 1 (4%) microbleed (Fig.5A–I). In addition, qualitative analysis after single-vessel tracing over several serial sections revealed that vessels involved in microbleeds were abnormally enlarged arterioles (sometimes showing microaneurysm-like features), were associated with fibrinoid necrotic changes, and extensive remodeling of the vessel wall extending upstream from the lesion site (Fig.7). Notably, on the same sections, several cortical vessels were observed (on average ~3 per H&E section) with the same pathological features (*i.e.* abnormally enlarged arterioles with fibrinoid necrotic changes, loss of SMCs and loss of Aβ from the wall) but without evidence of hemorrhage (Fig.7).

From the total number of 22 microinfarcts, in 13 (59%) the presumed culprit vessel(s) could be reliably identified. Vascular Aβ was observed at the core of 20 (91%) microinfarcts (p<0.001 compared to microbleeds), and for 18 (82%) Aβ was observed in the vessel wall upstream or downstream from the microinfarct. In 17 (77%) vessels fibrin(ogen) was present at the core of the microinfarct, but to a relatively mild degree in comparison to microbleeds. Intact SMCs at the lesion site were observed for only 2 (9%) microinfarcts (Fig.5J–R). In addition, qualitative analysis after single-vessel tracing over several serial sections revealed that vessels involved in microinfarcts appeared as intact arterioles but were presumably ‘stiff’ (*i.e.* heavily Aβ-occupied walls without SMCs) and with relatively narrow lumens (Fig.7).

Discussion

The results from this study revealed several main findings. First, we found that the number of microbleeds detected on *ex vivo* 3T MRI in cases with CAA correlated with the number of microbleeds observed on standard histopathological sections, whereas the number of microinfarcts did not. This suggests that MRI is sensitive for microbleed detection, but underestimates total microinfarct burden that is present throughout the brain. In fact, microinfarcts appear to greatly outnumber microbleeds in CAA cases. Second, we found that microbleeds and microinfarcts were not associated with CAA severity at the whole-hemisphere or regional level. Rather, microbleeds and microinfarcts are the results of

local changes, as the immediate surrounding local area of a microbleed contained fewer Aβ positive cortical vessels compared to simulated control lesions, whereas microinfarcts happened more often in local areas with an increased number of Aβ positive cortical vessels. Third, single-vessel tracing over serial sections revealed that microbleeds are associated with extensive vessel wall remodeling and loss of Aβ from a single vessel, whereas microinfarcts may be the result of increased Aβ and presumed vessel stiffening locally. These observations suggest that two distinct pathophysiological processes may lead to the formation of either hemorrhagic or ischemic lesions in CAA, and that microbleeds likely happen at a later timepoint in the disease process.

High-resolution *ex vivo* 3T MRI of intact hemispheres in this study detected approximately 2.5-times more microbleeds compared to microinfarcts across cases. In contrast, standard histopathology revealed 7-times more microinfarcts compared to microbleeds, which is in line with the previously reported high prevalence of microinfarcts as seen on pathology in CAA cases[14–16]. These observations strengthen the notion that microscopy has superior sensitivity compared to MRI for the detection of microinfarcts, as discussed elsewhere[5,10,17,18]. Whereas the number of microinfarcts detected on MRI did not correlate with the number of microinfarcts detected on histopathology in our study, the number of microbleeds did, confirming the previously reported finding that MRI is sensitive for microbleed detection, capable of capturing even the smallest hemorrhagic lesions[10]. The latter can be attributed to the fact that microbleeds benefit from a blooming effect owing to the high iron content in especially old microbleeds[12,19], whereas microinfarcts do not. Increasing MRI field strength (*e.g.* to 7T) may prove helpful to capture a wider spectrum of the total microinfarct burden in the brain.

At the population level the number of microbleeds on MRI correlated with Aβ burden as detected with positron emission tomography (PET) imaging[20]. Moreover, cortical florbetapir-PET levels were higher in patients with CAA-related acute ICH and lobar microbleeds compared to patients with hypertension-related acute ICH and deep microbleeds[21]. However, the correlation between microbleed numbers and Aβ levels within CAA cases has not been assessed to date, likely due to the relatively small number of patients that have undergone PET imaging[22]. Here, we confirmed the known predilection of microbleeds for posterior brain areas, which corresponded to greater CAA severity in parietal and occipital cortex. However, we did not find a strong relationship between the number of microbleeds and CAA severity at the whole-hemisphere or regional level. The absence of a significant correlation is unlikely due to the relatively small sample size, since we recently reported a significant correlation between microbleeds on *ex vivo* whole-hemisphere 3T MRI and cumulative fibrin(ogen) levels on histopathology[9]. The absence of a correlation between cortical microinfarcts and CAA severity at the whole-brain or regional level may be related to the poor detection of microinfarcts on MRI. Another explanation could be that although cortical microbleeds are rather specific for CAA, cortical microinfarcts have been associated with multiple etiologies, including non-small vessel disease related conditions such as atrial fibrillation[5].

At the local level, we reproduced the previously reported observation of fewer Aβ positive cortical vessels in the immediate surrounding area of a microbleed[7]. This contradicts a

widely held belief that bleeding happens as a direct result of increased CAA severity locally. A previous study found an increased Aβ burden in the immediate surrounding areas of microbleeds compared to simulated control lesions using PET imaging in patients with CAA[23,24]. An important difference between the PET study and our histopathology study is the resolution at which Aβ burden was assessed. Owing to the relatively low resolution of PET, shell sizes were set at 2 mm each, which is several magnitudes larger compared to the shell size in our study (360 μm in diameter). In contrast to microbleeds, we observed more Aβ positive cortical vessels in the immediate surrounding area of microinfarcts. A possible explanation for this observation could be that the extensive Aβ build-up in vessels surrounding an ischemic area is the result of impaired paravascular clearance of solutes, including Aβ, that occurs after vessel occlusions[25,26]. However, in our study we also found increased numbers of Aβ positive cortical vessels immediately surrounding recent/acute microinfarcts, which argues against the protein elimination failure hypothesis as an alternative explanation for our findings and suggests that microinfarcts do indeed occur in local areas with higher CAA severity.

Serial sectioning allowed us to make impactful observations at the single-vessel level. First, our findings provide evidence for a scenario in which microbleeds happen in unhealthy enlarged CAA-affected vessels due to Aβ-induced degeneration of SMCs, fibrin(ogen) build-up, extensive vessel wall remodeling, and loss of Aβ locally. The presence of several vessels on the microbleed-containing sections that had undergone very similar pathologic changes but had not ruptured provides further evidence for this scenario. Our findings also fit well with early observations of fibrinoid necrotic vessels and microaneurysms in brains with CAA-related hemorrhages[27] and more recently reported associations between microbleeds and fibrin(ogen) in patients with CAA[9]. Collectively, these data suggest that extensive build-up of Aβ in the walls of arterioles alone is not enough for the vessel to become fragile and rupture, but that it must undergo remodeling as well. This is in line with recent transcriptomic studies in patients with hereditary CAA (Dutch-type) that found upregulation of extracellular matrix-related pathways and TGFβ-induced pro-fibrotic genes[28,29]. Second, our findings provide evidence that microinfarcts happen in intact CAA-affected arterioles that are characterized by extensive Aβ build-up, loss of SMCs, and luminal narrowing. These vessels likely predispose to hypoperfusion and/or occlusions. We did not observe individual small thrombi or emboli in penetrating cortical arterioles that would have provided direct evidence for occlusion. However, our methods may not have been sensitive enough to detect (often temporary) small caliber vessel occlusions in 2D *post-mortem* tissue sections. The typical topographical distribution of microinfarcts in cortical areas that are perfused by end arteries points to hypoperfusion as another likely contributing mechanism for ischemia surrounding CAA-affected vessels [30–33]. Reduced vascular reactivity due to vessel stiffness in areas at risk of microinfarction may be an interesting early biomarker[34]. It is also possible that the single-vessel observations for microbleeds and microinfarcts reflect shared pathophysiological mechanisms that are captured at different timepoints in the evolution of the disease. This is supported by the observation that microinfarcts precede microbleeds on *in vivo* MRI in patients with Dutch-type CAA.[35] It may also explain the higher number of microinfarcts present in our CAA cases, which may have accumulated over a longer time-period. A major unanswered

question is why one affected vessel undergoes remodeling and another results in a microinfarct. Complex flow dynamics that differently affect separate locations within the larger connected vascular network likely play a role. Future experimental studies are needed to address this question in greater detail.

An important limitation of *post-mortem* studies is their cross-sectional nature, which makes it challenging to infer causes and consequences based on single neuropathological observations. An important alternative explanation for our observations is that bleeding from a vessel may result in loss of Aβ and vessel wall thickening, either directly or indirectly through local inflammatory responses. However, two important observations argue against this alternative explanation: 1) the absence of Aβ from walls that had recently (<24 hours) ruptured (Fig.5B C), because macrophages that take up red blood cells (and possibly Aβ) infiltrate the tissue >24 hours after a bleeding event, and 2) the presence of similarly abnormally enlarged vessels with fibrin(ogen) in the wall and reduced Aβ, but no evidence of bleeding (Fig.7). Because hemosiderin-containing macrophages remain present in the tissue for months up to years, it is most likely that these abnormal vessels without hemosiderin in the surrounding tissue represent vessels that had not bled. The observation of fibrin within astrocytes next to these vessels suggests that the blood-brain barrier was already compromised, rendering these abnormal vessels at risk for subsequent bleeding. Another limitation related to the nature of this autopsy study is the relative small number of cases that were included. Given the case-to-case variability, reflected in the wide range of detected lesions, it cannot be excluded that some cases contributed more than others to the observed associations. External validation in larger datasets therefore is preferred.

Our findings provide support for the notion that a single neuropathologic process, such as CAA, can produce two different types of lesions (*i.e.* hemorrhages and ischemic tissue injury), possibly by two distinct pathophysiological mechanisms. This framework has implications for other forms of cerebral small vessel diseases (such as hypertensive arteriopathy), for which CAA can provide a model to understand lesion formation. Our findings also have implications for anti-Aβ antibody trials suggesting that the removal of Aβ at a late disease stage from vessels that have already lost their SMCs and underwent extensive remodeling may increase the risk of bleeding. The focus should therefore be on early treatment to prevent extensive Aβ build-up in the walls of small vessels, thereby lowering the risk of lesion formation in patients with CAA or Alzheimer’s disease.

Acknowledgements

The authors would like to thank the families of the patients who generously donated their brains to our research studies. The authors would also like to thank Nathan Clement for his excellent assistance in the autopsy procedures. The work described in this study was supported by the National Institutes of Health [R01 NS096730, K99 AG059893, RF1 NS110054, and R21 AG046657] and the Netherlands Organization for Scientific Research [Rubicon fellowship 019.153LW.014 and Veni 91619021].

References

1. Greenberg SM, Charidimou A. Diagnosis of cerebral amyloid angiopathy: evolution of the Boston criteria. Stroke 2018;49:491–497 [PubMed: 29335334]
2. Greenberg SM, Vernooij MW, Cordonnier C, et al. Cerebral microbleeds: a guide to detection and interpretation. Lancet Neurol 2009;8:165–174 [PubMed: 19161908]

3. Reijmer YD, Fotiadis P, Martinez-Ramirez S, et al. Structural network alterations and neurological dysfunction in cerebral amyloid angiopathy. Brain 2015;138:179–188 [PubMed: 25367025]
4. Reijmer YD, Van Veluw SJ, Greenberg SM. Ischemic brain injury in cerebral amyloid angiopathy. J Cereb Blood Flow Metab 2016;36:40–54 [PubMed: 25944592]
5. Van Veluw SJ, Shih AY, Smith EE, et al. Detection, risk factors, and functional consequences of cerebral microinfarcts. Lancet Neurol 2017;16:730–740 [PubMed: 28716371]
6. Charidimou A, Boulouis G, Gurol ME, et al. Emerging concepts in sporadic cerebral amyloid angiopathy. Brain 2017;140:1829–1850 [PubMed: 28334869]
7. Van Veluw SJ, Kuijf HJ, Charidimou A, et al. Reduced vascular amyloid burden at microhemorrhage sites in cerebral amyloid angiopathy. Acta Neuropathol 2017;133:409–415 [PubMed: 27771772]
8. Van Veluw SJ, Reijmer YD, Van der Kouwe AJ, et al. Histopathology of diffusion imaging abnormalities in cerebral amyloid angiopathy. Neurology 2019; [Epub ahead of print]
9. Freeze WM, Bacskai BJ, Frosch MP, et al. Blood-brain barrier leakage and microvascular lesions in cerebral amyloid angiopathy. Stroke 2019;50:328–335 [PubMed: 30661497]
10. Van Veluw SJ, Charidimou A, Van der Kouwe AJ, et al. Microbleed and microinfarct detection in amyloid angiopathy: a high-resolution MRI-histopathology study. Brain 2016;139:3151–3162 [PubMed: 27645801]
11. Dale AM, Fischl B, Sereno MI. Cortical surface-based analysis. I. Segmentation and surface reconstruction. Neuroimage 1999;9:179–194 [PubMed: 9931268]
12. Van Veluw SJ, Biessels GJ, Klijn CJ, Rozemuller AJ. Heterogeneous histopathology of cortical microbleeds in cerebral amyloid angiopathy. Neurology 2016;86:867–871 [PubMed: 26843561]
13. Love S, Chalmers K, Ince P, et al. Development, appraisal, validation and implementation of a consensus protocol for the assessment of cerebral amyloid angiopathy in post-mortem brain tissue. Am J Neurodegener Dis 2014;3:19–32 [PubMed: 24754000]
14. Soontornniyomkij V, Lynch MD, Mermash S, et al. Cerebral microinfarcts associated with severe cerebral beta-amyloid angiopathy. Brain Pathol 2010;20:459–467 [PubMed: 19725828]
15. Kövari E, Herrmann FR, Hof PR, Bouras C. The relationship between cerebral amyloid angiopathy and cortical microinfarcts in brain ageing and Alzheimer's disease. Neuropathol Appl Neurobiol 2013;39:498–509 [PubMed: 23163235]
16. Ringman JM, Sachs MC, Zhou Y, et al. Clinical predictors of severe cerebral amyloid angiopathy and influence of APOE genotype in persons with pathologically verified Alzheimer disease. JAMA Neurol 2014;71:878–883 [PubMed: 24797962]
17. Westover MB, Bianchi MT, Yang C, Schneider JA, Greenberg SM. Estimating cerebral microinfarct burden from autopsy samples. Neurology 2013;80:1365–1369 [PubMed: 23486880]
18. Van Veluw SJ, Zwanenburg JJ, Engelen-Lee J, et al. In vivo detection of cerebral cortical microinfarcts with high-resolution 7T MRI. J Cereb Blood Flow Metab 2013;33:322–329 [PubMed: 23250109]
19. Schrag M, McAuley G, Pomakian J, et al. Correlation of hypointensities in susceptibility-weighted images to tissue histology in dementia patients with cerebral amyloid angiopathy: a postmortem MRI study. Acta Neuropath 2010;119:291–302 [PubMed: 19937043]
20. Graff-Radford J, Botha H, Rabinstein AA, et al. Cerebral microbleeds: Prevalence and relationship to amyloid burden. Neurology 2019;92:e253–262 [PubMed: 30568001]
21. Raposo N, Planton M, Péran P et al. Florbetapir imaging in cerebral amyloid angiopathy-related hemorrhages. Neurology 2017;89:697–704 [PubMed: 28724587]
22. Charidimou A, Farid K, Baron JC. Amyloid-PET in sporadic cerebral amyloid angiopathy: A diagnostic accuracy meta-analysis. Neurology 2017;89:1490–1498 [PubMed: 28855406]
23. Dierksen GA, Skehan ME, Khan MA et al. Spatial relation between microbleeds and amyloid deposits in amyloid angiopathy. Ann Neurol 2010;68:545–548 [PubMed: 20865701]
24. Gurol ME, Dierksen G, Betensky R, et al. Predicting sites of new hemorrhage with amyloid imaging in cerebral amyloid angiopathy. Neurology 2012;79:320–326 [PubMed: 22786597]
25. Garcia-Alloza M, Gregory J, Kuchibhotla KV, et al. Cerebrovascular lesions induce transient β-amyloid deposition. Brain 2011;134:3697–3707 [PubMed: 22120142]

26. Arbel-Ornath M, Hudry E, Eikermann-Haerter K, et al. Interstitial fluid drainage is impaired in ischemic stroke and Alzheimer's disease mouse models. Acta Neuropath 2013;126:353–364 [PubMed: 23818064]
27. Vonsattel JP, Myers RH, Hedley-Whyte ET. Cerebral amyloid angiopathy without and with cerebral hemorrhages: a comparative histological study. Ann Neurol 1991;30:637–649 [PubMed: 1763890]
28. Grand-Moursel L, Munting LP, Van der Graaf LM, et al. TGFβ pathway deregulation and abnormal phospho-SMAD2/3 staining in hereditary cerebral hemorrhage with amyloidosis-Dutch type. Brain Pathol 2018;28:495–506 [PubMed: 28557134]
29. Grand-Moursel L, Van Roon-Mom WMC, Kielbasa SM, et al. Brain transcriptomic analysis of Hereditary Cerebral Hemorrhage With Amyloidosis-Dutch type. Front Aging Neurosci 2018;10:102 [PubMed: 29706885]
30. Suter OC, Sunthorn T, Kraftsik R, et al. Cerebral hypoperfusion generates cortical watershed microinfarcts in Alzheimer disease. Stroke 2002;33:1986–1992 [PubMed: 12154250]
31. Okamoto Y, Yamamoto T, Kalaria RN, et al. Cerebral hypoperfusion accelerates cerebral amyloid angiopathy and promotes cortical microinfarcts. Acta Neuropathol 2012;123: 381–394 [PubMed: 22170742]
32. Van Veluw SJ, Hilal S, Kuijf HJ, et al. Cortical microinfarcts on 3T MRI: Clinical correlates in memory-clinic patients. Alzheimers Dement 2015;11:1500–1509 [PubMed: 25956990]
33. Kapasi A, Leurgans SE, James BD, et al. Watershed microinfarct pathology and cognition in older persons. Neurobiol Aging 2018;70:10–17 [PubMed: 29935416]
34. Dumas A, Dierksen GA, Gurol ME, et al. Functional magnetic resonance imaging detection of vascular reactivity in cerebral amyloid angiopathy. Ann Neurol 2012;72:76–81 [PubMed: 22829269]
35. Van Rooden S, Van Opstal AM, Labadie G, et al. Early magnetic resonance imaging and cognitive markers of hereditary cerebral amyloid angiopathy. Stroke 2016;47:3041–3044. [PubMed: 27834748]
36. Hyman BT, Phelps CH, Beach TG, et al. National Institute on Aging-Alzheimer's Association guidelines for the neuropathologic assessment of Alzheimer's disease. Alzheimers Dement 2012;8:1–13 [PubMed: 22265587]

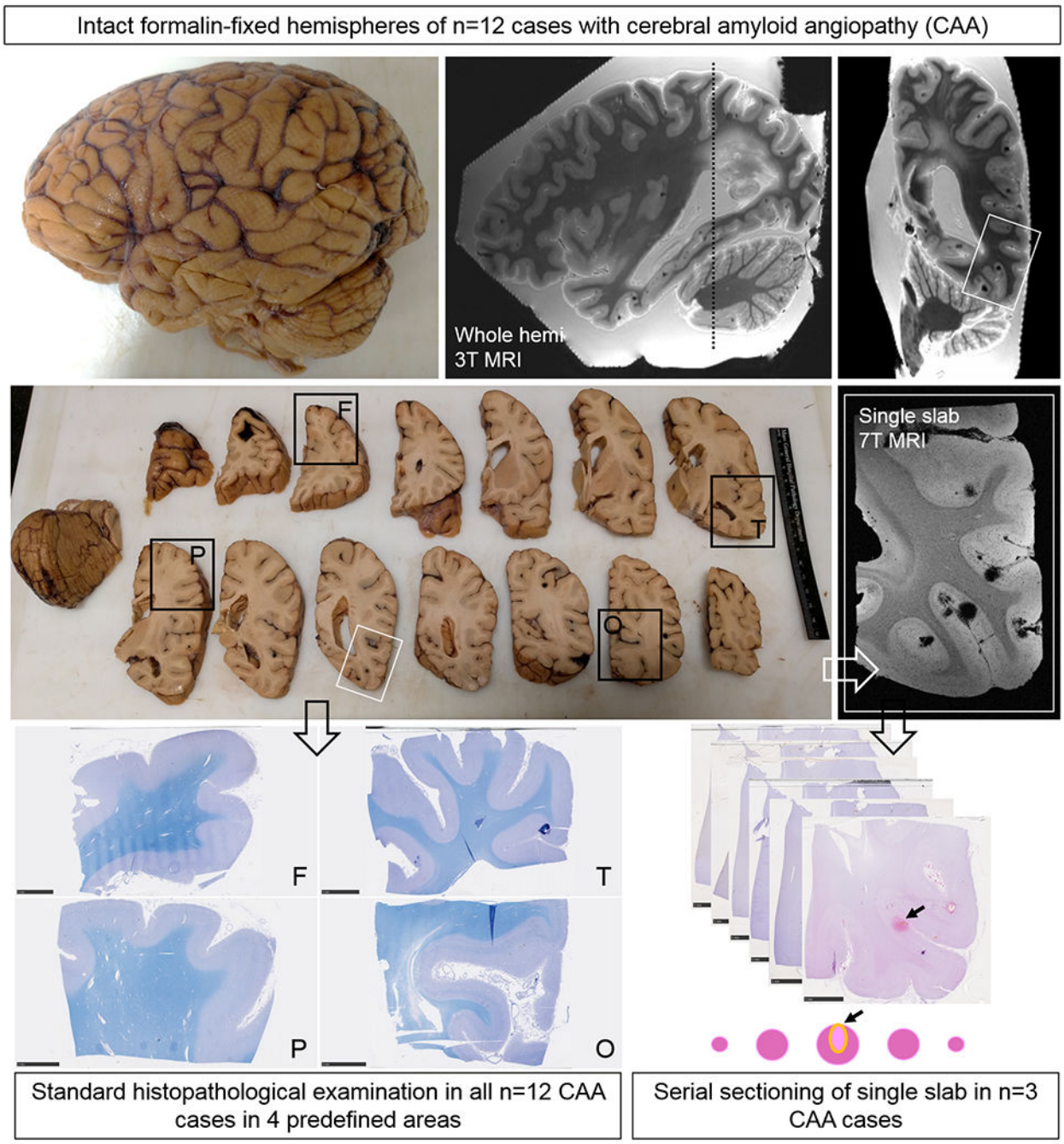

Figure 1.

Study design.

Intact formalin-fixed hemispheres of 12 CAA cases were subjected to high-resolution *ex vivo* 3T MRI to detect microbleeds and microinfarcts. Next, the hemispheres were cut in 10 mm-thick coronal slabs and samples were taken from pre-defined standard areas of frontal (F), temporal (T), parietal (P), and occipital (O) cortex, to fit a standard tissue cassette (black squares). Four adjacent 6 μm-thick sections were cut from these samples and stained with hematoxylin & eosin (H&E) or Luxol fast blue H&E (depicted here) and underwent

immunohistochemistry to detect Aβ and GFAP. Finally, three additional samples were taken from three cases in an area with multiple microbleeds (n=2, from temporal cortex) or microinfarcts (n=1, from parieto-occipital cortex) guided by the *ex vivo* 3T MR images (white square). These samples underwent ultra-high-resolution *ex vivo* 7T MRI scanning to confirm the high number of lesions in those areas. After 7T MRI, the samples were cut in half to fit two standard tissue cassettes and underwent complete serial sectioning. Sections 1, 21, 41, 61 etc. were stained with H&E to identify microbleeds and microinfarcts, and sections 2, 6, 10, 14 etc. underwent immunohistochemistry against Aβ. If present, the vessel that could be traced through the core of the lesion was identified as the presumed culprit vessel. In addition, for each identified lesion on H&E, sections adjacent to a microbleed or microinfarct underwent immunohistochemistry to detect fibrin(ogen) or SMCs.

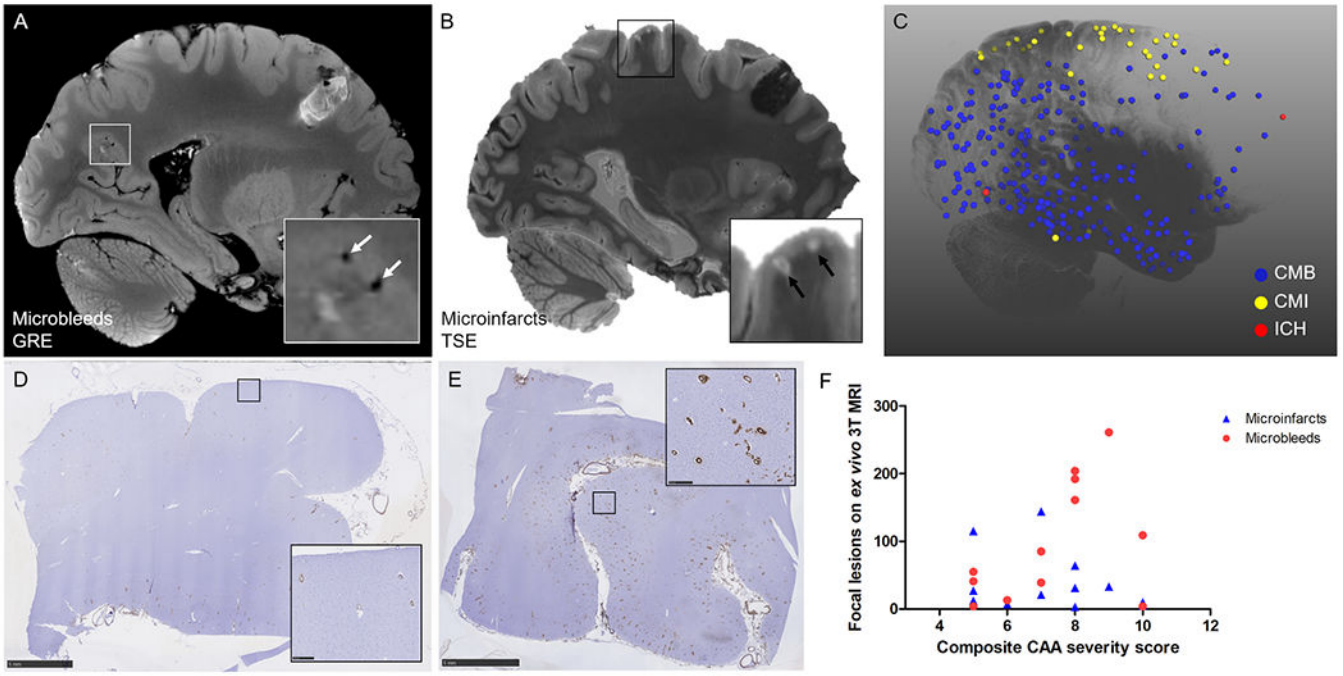

Figure 2.

Whole-brain associations of microbleeds and microinfarcts with CAA severity. Cortical microbleeds were assessed on the *ex vivo* 3T MRI gradient-echo (GRE) scans (A) and cortical microinfarcts on the *ex vivo* 3T MRI T2-weighted turbo-spin echo (TSE) scans (B). The projection of annotated lesions on a 3D reconstruction of a representative hemisphere (case #2) demonstrates that microbleeds (CMB, blue dots) were more often observed in posterior parts of the brain, whereas microinfarcts (CMI, yellow dots) frequently involved the areas of the brain perfused by end arteries (C). Note: red dots are areas affected by intracerebral hemorrhages (ICH). CAA severity was assessed on standard sections from frontal (D, example of score 1), temporal, parietal, and occipital (E, example of score 3) cortex to create a composite CAA severity score. Neither the number of microbleeds (red circles, Spearman's ρ 0.426, p=0.17) nor the number of microinfarcts (blue triangles, Spearman's ρ −0.278, p=0.38) were associated with composite CAA severity score (F). Scale bar in D and E = 5 mm.

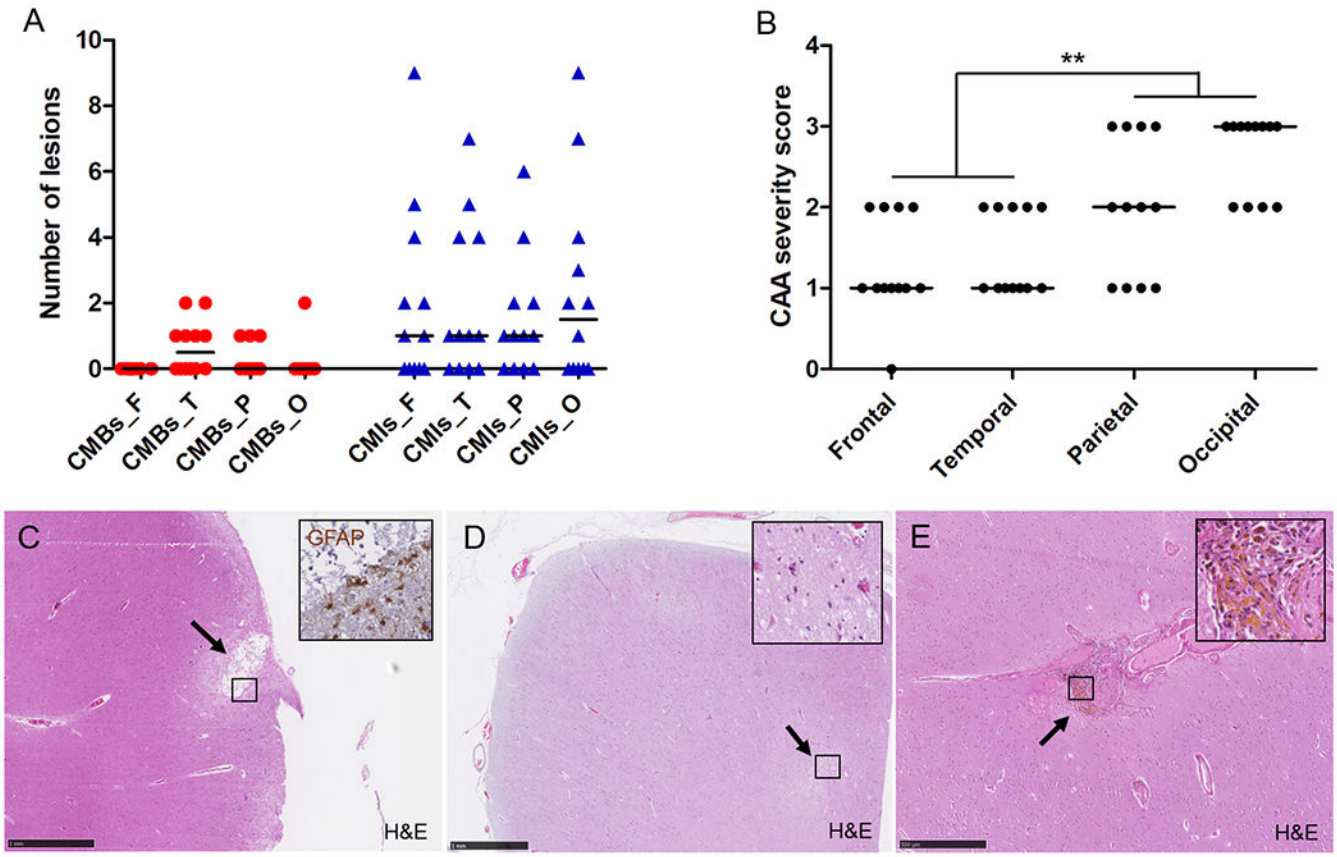

Figure 3.

Regional associations on standard histopathologic examination of microbleeds and microinfarcts with CAA severity.

On average, CAA severity across all 12 cases followed an anterior-to-posterior distribution (B), whereas number of histopathologically-observed microbleeds and microinfarcts did not (A), explaining weak regional associations. From the total number of 94 microinfarcts observed on standard histopathology, 61 (65%) were considered old/chronic based on GFAP positivity (inset) (C, this example follows the perfusion area of a penetrating cortical vessel) and 33 (35%) recent/acute based on the presence of ‘red’ neurons (inset) (D, this example is located deeper (within cortical layer III-VI)). From the total number of 13 microbleeds observed on standard histopathology, 12 (92%) were considered old/chronic based on the presence of hemosiderin-containing macrophages (inset) (E), and 1 (8%) recent/acute (not shown). Median is indicated in A and B. Scale bar in C and D = 1 mm, scale bar in E = 500 μm.

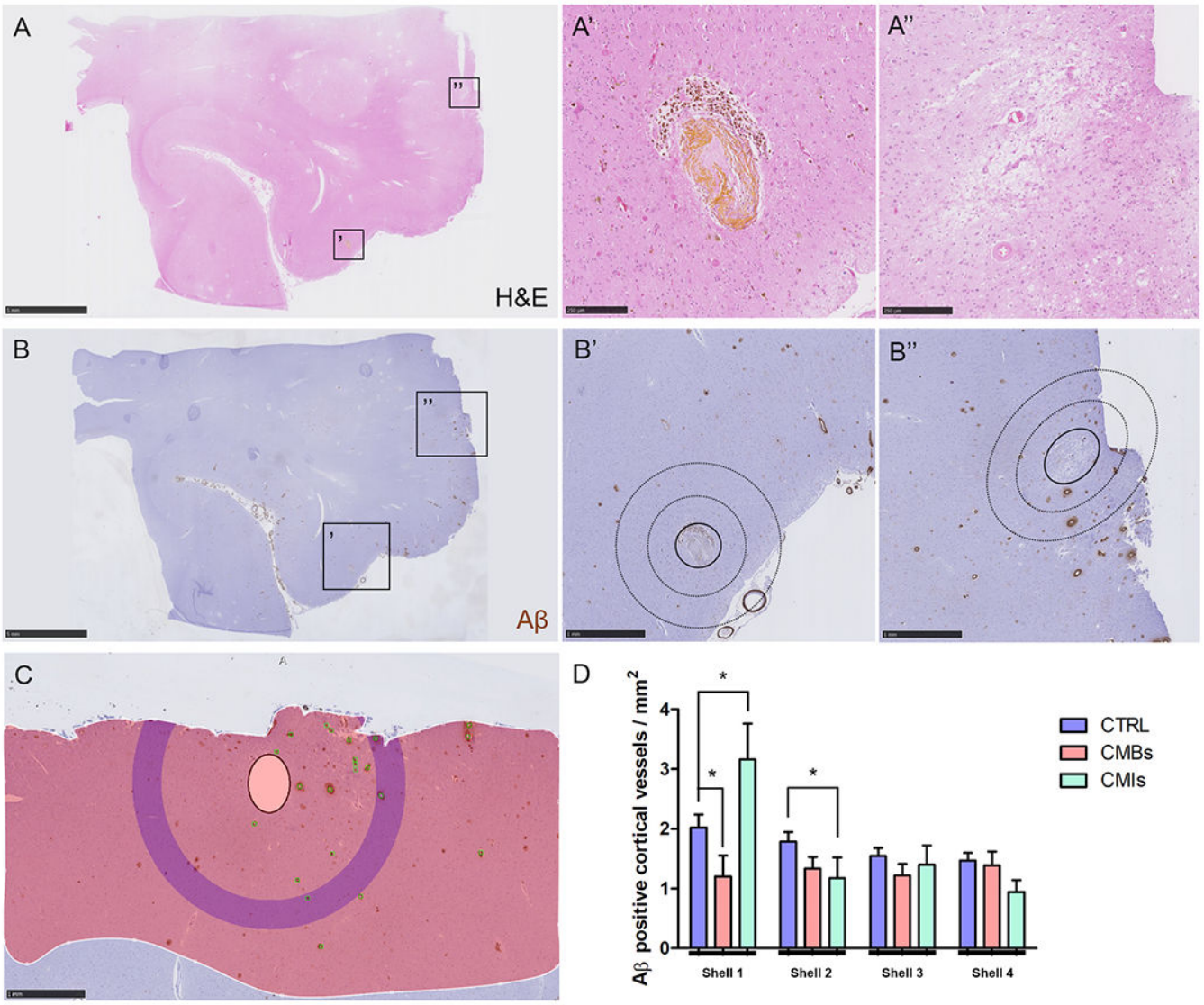

Figure 4.

Local associations of microbleeds and microinfarcts with Aβ positive cortical vessels. Based on the H&E-stained serial sections (A) from the additional samples taken from the temporal cortex in two CAA cases, 28 microbleeds (A') and 18 microinfarcts (A'') were included. Lesions were localized on the adjacent Aβ-stained sections (B) to perform Sholl analysis (B'B'', inner circle with solid outline indicates masked area, circles with dotted outlines indicate first two shells). After masking of the lesion, Aβ positive cortical vessels were manually annotated (green markers), the cortical ribbon was outlined (red shaded area), and the density of Aβ positive cortical vessels was generated by the software for four concentric circles extending from the outer border of the masked area (C, purple concentric circle in this example is shell 4). Significantly fewer Aβ positive cortical vessels were observed in the first shell immediately adjacent to a microbleed compared to a simulated control lesion (p=0.023), whereas more Aβ positive cortical vessels were observed in the first shell immediately adjacent to a microinfarct compared to a simulated control lesion

(p=0.054) (D). For the second shell significantly fewer Aβ positive cortical vessels were observed for microinfarcts compared to simulated control lesions (p=0.039). Scale bar in A and B = 5 mm, scale bar in B', B'', and C = 1 mm, scale bar in A' and A'' = 250 μm. Error bars in D = SEM.

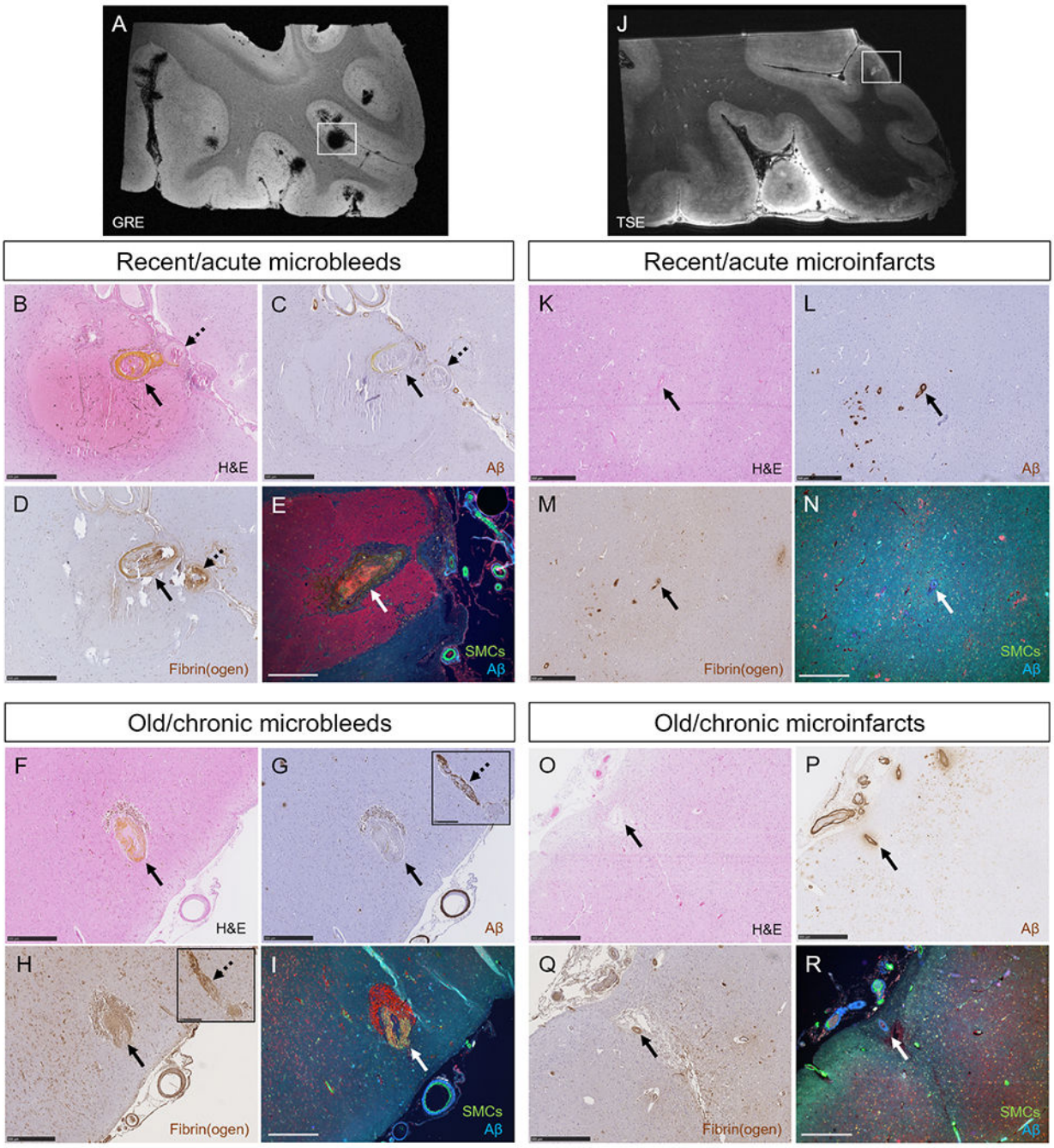

Figure 5.

Single-vessel pathologies of microbleeds and microinfarcts.

The high numbers of microbleeds in the additional samples taken from the temporal cortex in two CAA cases were confirmed with *ex vivo* 7T MRI (A). Single-vessel analysis on serial sections revealed for recent/acute microbleeds: absence of Aβ from the vessel wall at the site of bleeding (BC, arrow, yellow substance is hematoidin). In this example also no Aβ was observed upstream from the bleeding site (C, broken arrow). Extensive fibrin(ogen) was observed at the rupture site and upstream (D). No intact SMC was observed in the

responsible vessel (E). Similar observations were made for old/chronic microbleeds (F, brown deposits are hemosiderin-containing macrophages). Note that for this example, Aβ was not present at the rupture site (G, arrow), but was observed downstream (G, broken arrow, inset shows the same vessel captured on a consecutive serial section). Extensive fibrin(ogen) was observed both at the rupture site (H, arrow) and downstream (H, broken arrow, inset shows the same vessel captured on a consecutive serial section), but no SMCs (I). The high number of microinfarcts in the additional sample taken from the parieto-occipital cortex in one CAA case was confirmed with *ex vivo* 7T MRI (J). Single-vessel analysis on serial sections revealed for recent/acute microinfarcts (K): presence of Aβ in the wall(s) of vessel(s) at the core of the lesion (L), mild fibrin(ogen) deposition (M), and loss of SMCs (N). Similar observations were made for old/chronic microinfarcts (O-R). All scale bars are 500 μm. Note that the lesion in panel E is a different recent/acute microbleed than in panel B, C, and D.

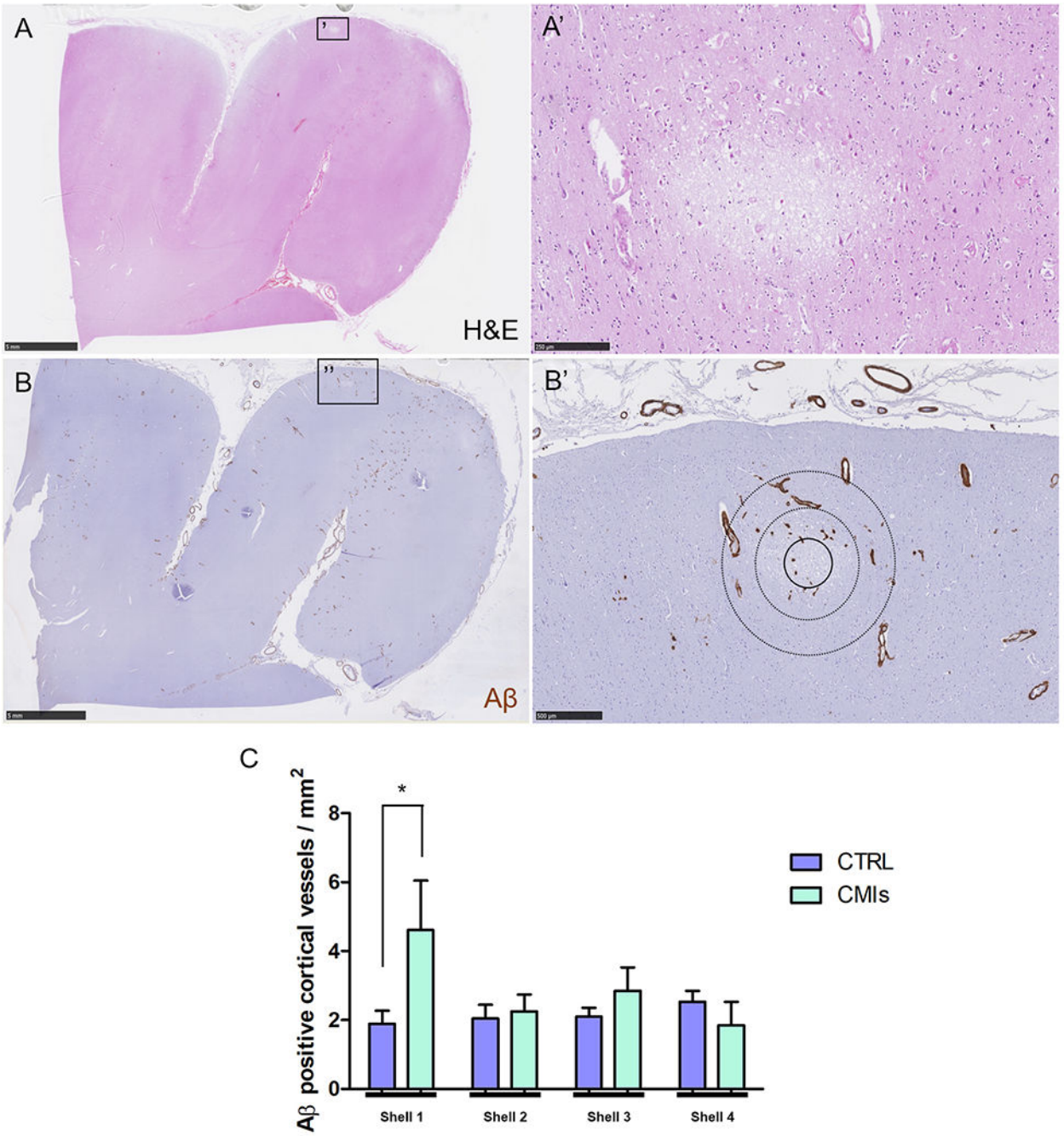

Figure 6.

Local associations of recent/acute microinfarcts with Aβ positive cortical vessels. Based on the H&E-stained serial sections (A) from the third additional sample taken from the parieto-occipital cortex in one CAA case, 11 recent/acute microinfarcts (A') were included. Lesions were localized on the adjacent Aβ-stained sections (B) to perform Sholl analysis (B', inner circle with solid outline indicates masked area, circles with dotted outlines indicate first two shells). Significantly more Aβ positive cortical vessels were observed in the first shell immediately adjacent to a microinfarct compared to a simulated

control lesion (p=0.031) (C). Scale bar in A and B = 5 mm, scale bar in A’ = 250 μm, scale bar in B’ = 500 μm. Error bars in C = SEM.

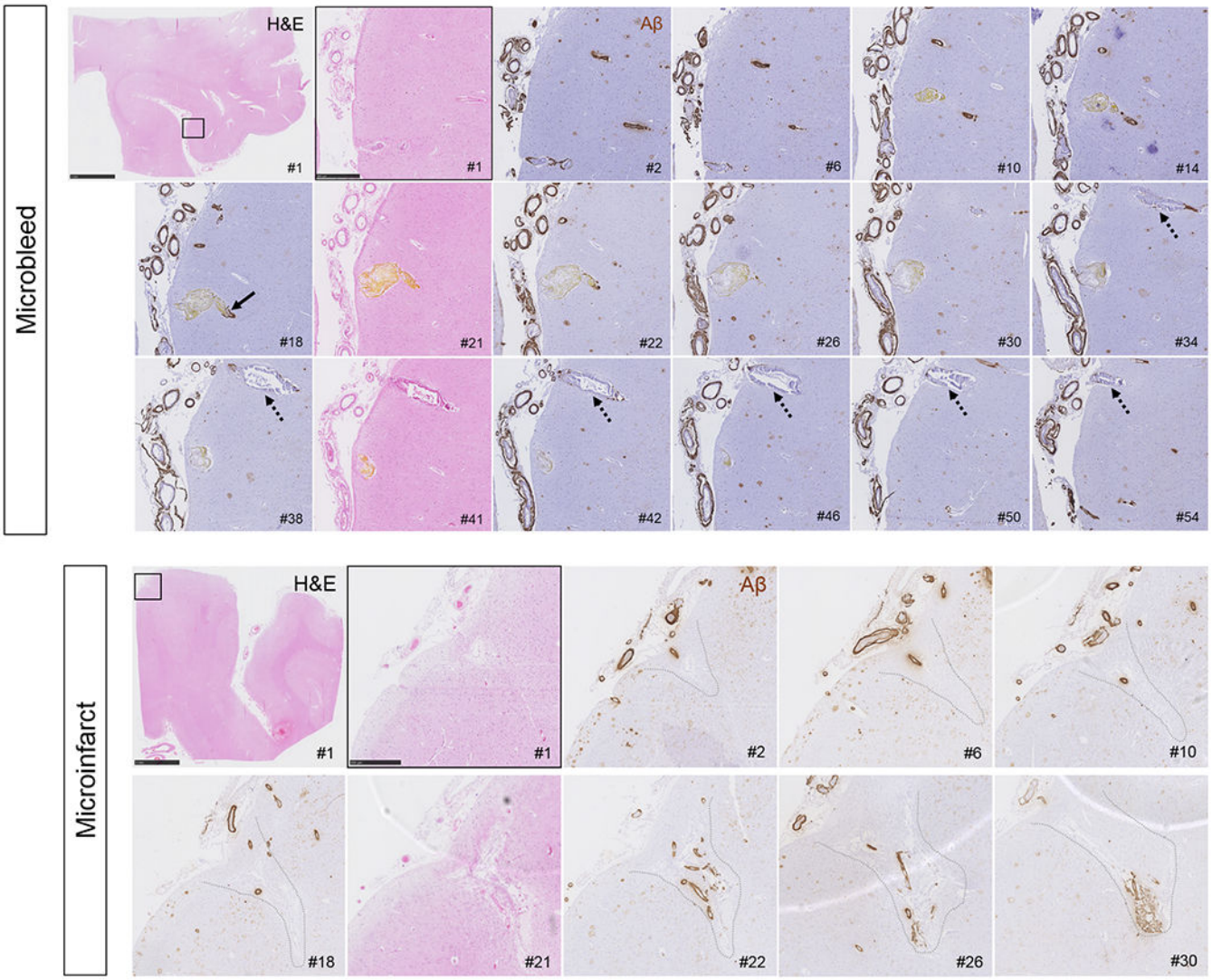

Figure 7.

Serial H&E and Aβ stained sections capturing a recent/acute microbleed and an old/chronic microinfarct.

Vessels responsible for microbleeds were traced on serial sections, stained with H&E (#1, 21, 41 etc.) and Aβ (#2, 6, 10 etc.) and revealed absence of Aβ at the rupture site, but subtle Aβ upstream and downstream (arrow). This example is a recent/acute microbleed characterized by hematoidin (yellow substance). Note that the vessel is enlarged at the site of bleeding (section #21). Moreover, this vessel did not have any SMCs left but showed extensive fibrin(ogen) build-up in the wall (not shown). Note the vessel that runs in parallel to the microbleed (broken arrows), which is also abnormally enlarged and shows loss of Aβ from the vessel wall but has not ruptured. Scale bar in first panel = 5 mm, scale bar in second panel = 500 μm. Microinfarcts were traced on serial sections, stained with H&E (#1, 21, 41 etc.) and Aβ (#2, 6, 10 etc.), which revealed extensive vascular Aβ at the core of the microinfarcts, as well as upstream and downstream. This example is a chronic/old microinfarct characterized by tissue loss, cavitation, and GFAP positivity (not shown). Note

that the walls of the vessels at the core of the microinfarct appear relatively intact, except that they lost their SMCs (not shown). Scale bar in first panel = 5 mm, scale bar in second panel = 500 μm.

Table 1.

Case characteristics and *ex vivo* MRI and neuropathological findings.

Case ID / sex / hemisphere	Age at death (years) / death due to acute ICH	PMI (hours)	CMBs on *ex vivo* 3T MRI / CMIs on *ex vivo* 3T MRI	CAA severity (cum score)*	Other neuropathological observations#
1 / M / R	80 / N	Unk	41 / 115	5	A3B3C2
2 / M / L	70 / Y	16	261 / 33	9	A3B3C1, moderate hypertensive vasculopathy
3 / M / R	76 / N	27	39 / 21	7	A3B3C2, arteriolosclerosis
4 / M / L	65 / Y	14	85 / 144	7	A3B1C2
5 / M / R	81 / N	Unk	4 / 12	5	A3B2C2, moderate arteriolosclerosis
6 / F / L	70 / n/a	Unk	13 / 7	6	n/a
7 / M / L	67 / N	Unk	109 / 10	10	A3B3C2
8 / M / L	69 / Y	36	4 / 5	10	A3B1C2, mild arteriolosclerosis
9 / F / R	64 / Y	30	161 / 3	8	A3B2C3
10 / F / R	79 / Y	37	204 / 31	8	A3B3C2
11 / M / L	67 / N	24	55 / 27	5	A3B1C1, moderate arteriolosclerosis
12 / F / L	88 / Y	11	192 / 64	8	A2B3C2

*CAA severity was evaluated on the Aβ-stained sections from the pre-defined standard areas of frontal, temporal, parietal, and occipital cortex using a 4-point scale; absent (0), scant Aβ deposition (1), some circumferential Aβ (2), widespread circumferential Aβ (3), following proposed consensus criteria[13]. Scores from the four areas were added to form a cumulative CAA severity score.

#Extracted from neuropathology reports, based on routine neuropathological examination. ABC score reflects the NIA-Alzheimer Association score for Alzheimer's Disease neuropathologic changes[36].

ICH: intracerebral hemorrhage, PMI: *post-mortem* interval, CMBs: cerebral microbleeds, CMIs: cerebral microinfarcts, CAA: cerebral amyloid angiopathy, M: male, F: female